Current Applied Physics 20 (2020) 489–497

Contents lists available at ScienceDirect

Current Applied Physics

journal homepage: www.elsevier.com/locate/cap

ITO/Au/ITO multilayer thin films on transparent polycarbonate with enhanced EMI shielding properties

Nursev Erdogan[a,*], Fuat Erden[a,b], A. Taner Astarlioglu[a], Mehtap Ozdemir[c], Salih Ozbay[a], Gulnur Aygun[d], Lutfi Ozyuzer[c,d]

[a] Turkish Aerospace, Advanced Material, Process and Energy Technology Center, 06980, Ankara, Turkey
[b] Sivas University of Science and Technology, Department of Aeronautical Engineering, 58050, Sivas, Turkey
[c] Teknoma Technological Materials Inc. Izmir Technology Development Zone, Urla, 35430, Izmir, Turkey
[d] Izmir Institute of Technology, Department of Physics, Urla, 35430, Izmir, Turkey

ARTICLE INFO

Keywords:
Transparent conductive oxide
Multilayer thin films
Sputtering
Electromagnetic interference shielding
Indium-tin oxide
Gold

ABSTRACT

ITO/Au/ITO multilayer thin films were deposited onto polycarbonate substrate via magnetron sputtering technique without intentional heating. The deposition times of both ITO and Au layers were studied to optimize the overall transparency and conductivity. As-prepared thin films were characterized using X-ray diffraction analysis, secondary ion mass spectroscopy, scanning and transmission electron microscopy, atomic force microscopy and physical property measurement system. The optical measurement results revealed that the transmittance of the films were enhanced by increasing the gold deposition time up to 15 s. Beyond this point, further increasing the duration caused a decrease in optical transmittance. Upon optimization of the Au deposition time, the deposition duration of ITO layers was also studied to increase electromagnetic interference (EMI) shielding effectiveness (SE). Maximum EMI SE in this work was measured as 26.8 dB, yielding 99.8% power attenuation, which was verified by simulation results.

1. Introduction

Transparent conducting oxide (TCO) films play a key role in a number of applications including displays, smart windows, solar cells, photodetectors, electroluminescence devices and organic light emitting diodes [1,2], IR-reflective coatings [3], heatable layers in defrosting windows [4] and dissipating static charge [5,6]. To date, various alternative TCOs such as indium tin oxide (ITO) [7], indium zinc oxide (IZO) [8], gallium zinc oxide (GZO) [9] and aluminum zinc oxide (AZO) [10,11] have been proposed to be used in these applications. Among all alternatives, ITO dominates the field due to its performance in high visible region transmission and low resistivity [7].

Thermoplastic polymers are used in many industrial applications due to their impact resistance, toughness, durability and price advantage. However, they do not withstand the temperatures required for some widely used deposition steps in semiconductor processing. Magnetron sputtering with a heat treatment is the most common deposition method for semiconductor processing, as it allows large scale deposition [12]. However, heating is not applicable when the substrate is a thermoplastic material. Therefore, in the case of thermoplastic substrates, the electrical and optical properties should be improved by other means, rather than improving crystallinity via substrate heating [13]. One of the most effective ways to realize improved optical transmission and electrical conductivity is to use sandwich type structures such as dielectric/metal/dielectric (D/M/D) multilayer films [14]. In this structure, a very thin metal film is embedded as an interlayer to improve the electrical conductivity without deteriorating the transparency of the dielectric material. Metals such as Au, Ag, Cu, Al and their alloys have been extensively studied for interlayer of D/M/D films [15]. While the surface of other metals is easily altered in air/moisture environments due to the formation of oxides, gold retains its shiny aspect over time because gold oxides are not stable [16]. It is already reported that the sheet resistance of sandwich structures including Au interlayer remains constant for an exposure time of 600 h at 60 °C, in air having a relative humidity of 90% [13].

Regarding to the quality of a thin metal interlayer between dielectric components, the fabrication process generally gives rise to aggregated gold islands before a homogeneous layer is deposited [17]. Sytchkova et al. [18] and Guske et al. [19] both reported that the thickness of metal film should exceed 10 nm to prevent discontinuity of the interlayer coat. Based upon this limitation, numerical studies have been conducted to obtain the best thickness values of individual layers

* Corresponding author.
E-mail address: nursev.erdogan@tai.com.tr (N. Erdogan).

https://doi.org/10.1016/j.cap.2020.01.012
Received 15 November 2019; Received in revised form 30 December 2019; Accepted 20 January 2020
Available online 23 January 2020

with further correlation with experimental studies [20]. Although plenty of work has been done on flexible substrates [13,21], research towards robust thin film deposition onto structural polymer substrates is very limited. Especially, a sandwich structure on polymer substrates consisting of a metal interlayer between TCO layers, providing optimum optical transparency and electrical conductivity with a focus on effective EMI shielding remains elusive.

In this work, ITO/Au/ITO multilayer films were systematically deposited on polycarbonate (PC) and Soda Lime Glass (SLG) substrates using magnetron sputtering technique. The deposition times of Au and ITO layers were optimized to provide highest electrical conductivity and visible light transparency. The structural, electrical, and optical properties of the sandwich films were studied and the EMI shielding behavior of the D/M/D films were evaluated via both numerical and experimental methods. Through a detailed study on the factors influencing EMI shielding performance like individual film thicknesses and electrical conductivity, as well as carrier mobility and carrier concentration, the maximum shielding effectiveness of about 26.8 dB at 8–12 GHz, providing 99.8% power attenuation could be achieved by ITO/Au/ITO multilayer thin films.

2. Material and methods

2.1. Deposition of multilayer films

Deposition of ITO and Au thin films were performed in a magnetron sputtering system that was equipped with two cathodes [22]. DC power was applied to both ITO and Au targets. The ITO target used in this work was an In_2O_3 (90%) and SnO_2 (10%) containing disc with 2 in. diameter and 0.25 in. thickness. A 99.99% pure disk with 2 in. diameter and 0.0625 in. thickness was used as gold target for interlayer deposition. ITO bi-layer and ITO/Au/ITO trilayer films were deposited on Soda Lime Glass (SLG, 1 cm x 1 cm x 1 mm) and Makrolon® clear polycarbonate sheet (PC, ASTM D1746 Haze value 1, 50 mm × 50 mm x 21 mm) substrates at room temperature (RT) without intentional substrate heating. They were then cut into smaller pieces with different geometries using Dicing Saw and CNC machine for characterization purposes. The substrates were ultrasonically cleaned in methanol and deionized water for 20 min, respectively, and subsequently dried with a flow of nitrogen. Moreover, the substrates were plasma treated to increase the hydrophilicity on the surface under pure O_2 gas. The contact angle measurements of substrates before and after plasma treatment is shown in Table S1. Prior to deposition, the chamber was evacuated to a pressure less than $2x10^{-6}$ Torr. Then, the target was pre-sputtered for 5 min to remove the contaminants. The sputtering was performed at $\sim 3x10^{-3}$ Torr under pure Ar gas (40 sccm). In the first set of experiments, initial ITO layer was deposited onto SLG and PC substrates for 7 min, while keeping the distance between target and substrate constant. After that, Au was deposited on the ITO for various durations as given in Table 1. It should be noted that Au deposition duration was controlled using a pneumatic shutter driven by computer for precise timing. Finally, ITO top-layer was deposited onto Au layer for 7 min. The second set of specimens were prepared by changing the deposition time of ITO and keeping the best value of Au deposition time as constant at 15 s (see Table 1). The applied power on ITO and Au targets

Table 1
Deposition times of the ITO/Au/ITO multi-layer thin films onto SLG and PC substrates.

Coding	ITO deposition time (min)	Au deposition time (s)	ITO deposition time (min)
7-0-7	7	0	7
7-3-0	7	3	0
7-3-7	7	3	7
7-7-7	7	7	7
7-11-7	7	11	7
7-13-7	7	13	7
7-15-7	7	15	7
7-17-7	7	17	7
6-15-6	6	15	6
8-15-8	8	15	8

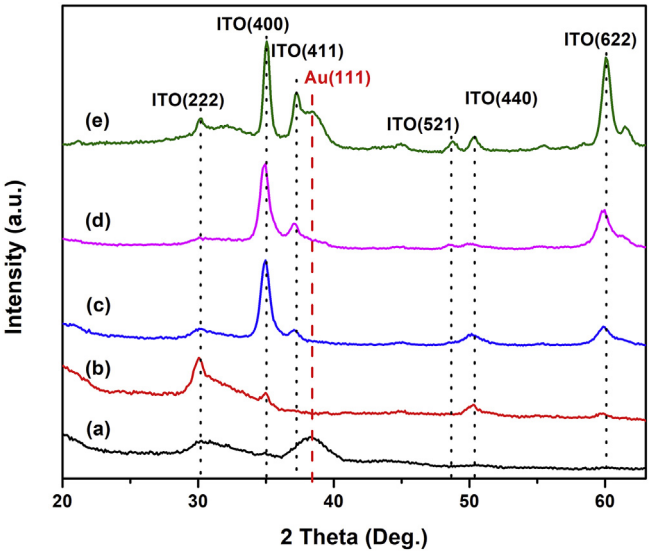

Fig. 1. GIXRD patterns of representative samples (a) 7-3-0, (b)7-0-7, (c)7-3-7, (d)7-11-7 and (e) 7-15-7.

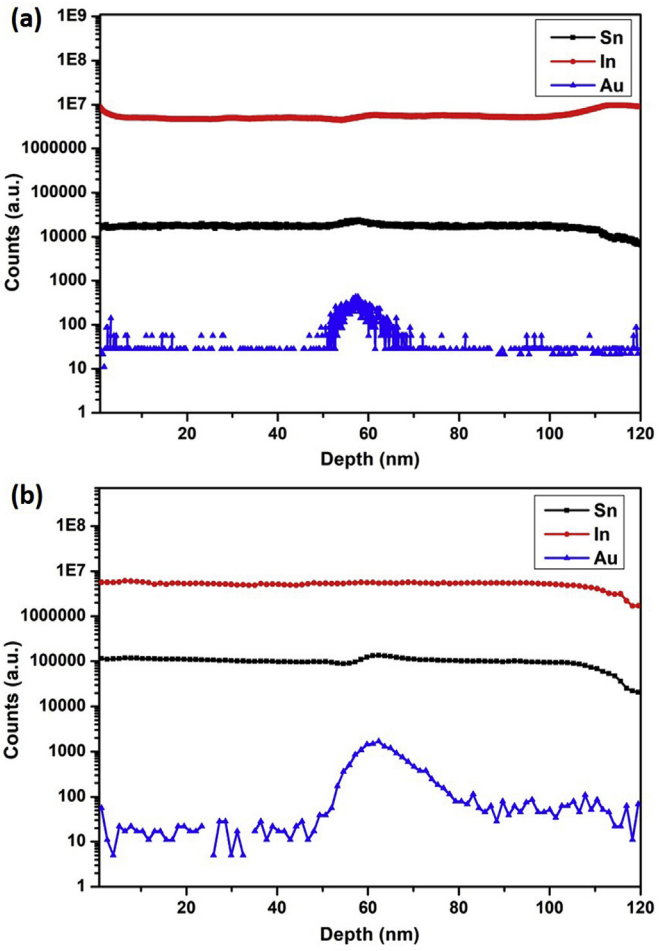

Fig. 2. SIMS analyses of samples (a) 7-3-7 and (b) 7-15-7.

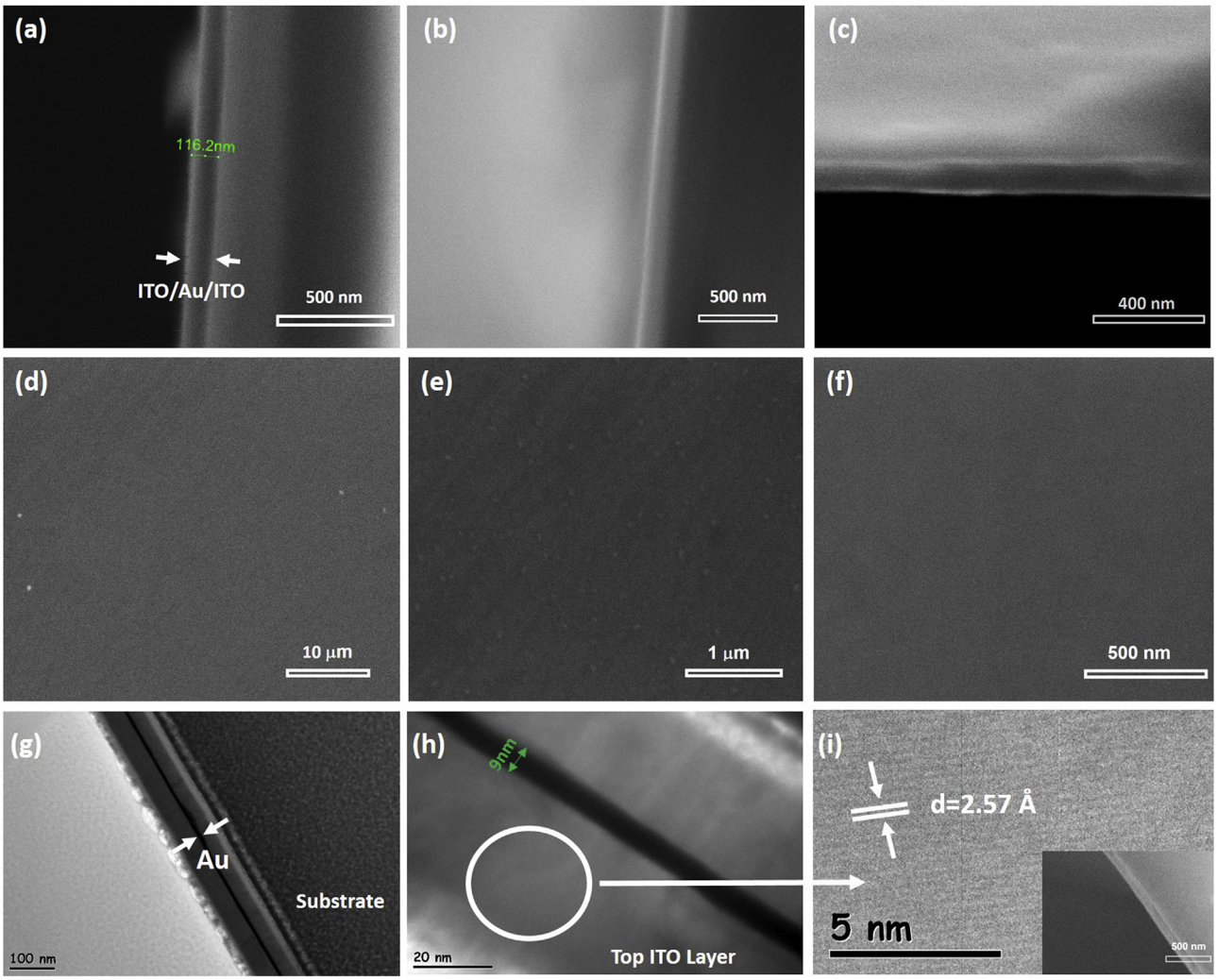

Fig. 3. Representative cross section FESEM images of samples (a) 7-7-7, (b) 7-15-7, (c) 8-15-8, surface FESEM images of samples (d) 7-7-7, (e) 7-15-7, (f) 8-15-8 and (g)–(i) HRTEM images of sample 6-15-6 with several magnifications. Inset shows cross section FESEM image of sample 6-15-6.

during depositions were 20 and 15 W, respectively. The sample coding and deposition times of Au and ITO layers are listed in Table 1.

2.2. Characterization

2.2.1. Material characterization

Grazing incidence X-Ray Diffraction (GIXRD) was carried out in the Grazing focusing geometry at a grazing angle of the incident X-ray beam (ω) 0.7° using a Panalytical X-Ray Diffractometer, with Cu-Kα radiation (λ = 1.5406 Å). XRD patterns were recorded from 2θ = 20–60° with a step size of 0.016° for all samples. Secondary Ion Mass Spectroscopy (SIMS) was conducted using an oxygen gun with an emission of 10.00 mA. A Veeco DEKTAK 150 profilometer was used to determine the thickness of the films. The average roughness measurements were performed on 10 μm × 10 μm areas with tapping mode of AFM-Asylum under ambient conditions. Surface and cross sectional morphologies of films were analyzed using FESEM and HRTEM analyses (Jeol, NanoSEM and HRTEM). HRTEM samples were prepared by Focused Ion Beam (FIB) lithography, as shown in Fig. S1.

2.2.2. Optical and electrical characterization

Optical properties of the multilayer films were investigated by optical transmittance measurements in 200–2500 nm wavelength range, using a PerkinElmer Lambda 950 UV/VIS/NIR spectrophotometer. Electrical measurements including conductivity, sheet resistance, charge carrier concentration and carrier mobility were conducted using a Cryogenic Physical Property Measurement System (PPMS).

2.2.3. Electromagnetic characterization

The EMI shielding effectiveness (SE) was tested using the ASTM (American Society for Testing and Materials) D5568 method [23] using a Network Analyzer (Keysight, former Agilent Technologies) with a waveguide method. Measured frequencies ranged from 8.2 GHz to 12 GHz. EMI-SE values in terms of decibels (dB) were calculated using the following equations:

$$EMI\ SE\ (dB) = -10log_{10}(P_T/P_I) \quad (1)$$

$$EMI\ SE\ (dB) = -20log_{10}\left(\frac{1}{|S_{21}|}\right) \quad (2)$$

where dB is the unit of the power ratio, which is typically used to specify the shielding effectiveness, and P_T and P_I indicate the power of the transmitted and incident electromagnetic (EM) waves, respectively.

Moreover, the S_{21} parameters of the structures were also theoretically calculated through CST Microwave Studio to compare the experimental findings with simulation results. In terms of boundary conditions, the electric field intensity at the sides and magnetic field intensity at the top and bottom surfaces were set to zero for correctly simulating the experimental setup. Besides, open boundary conditions were employed along the propagation direction of the electromagnetic

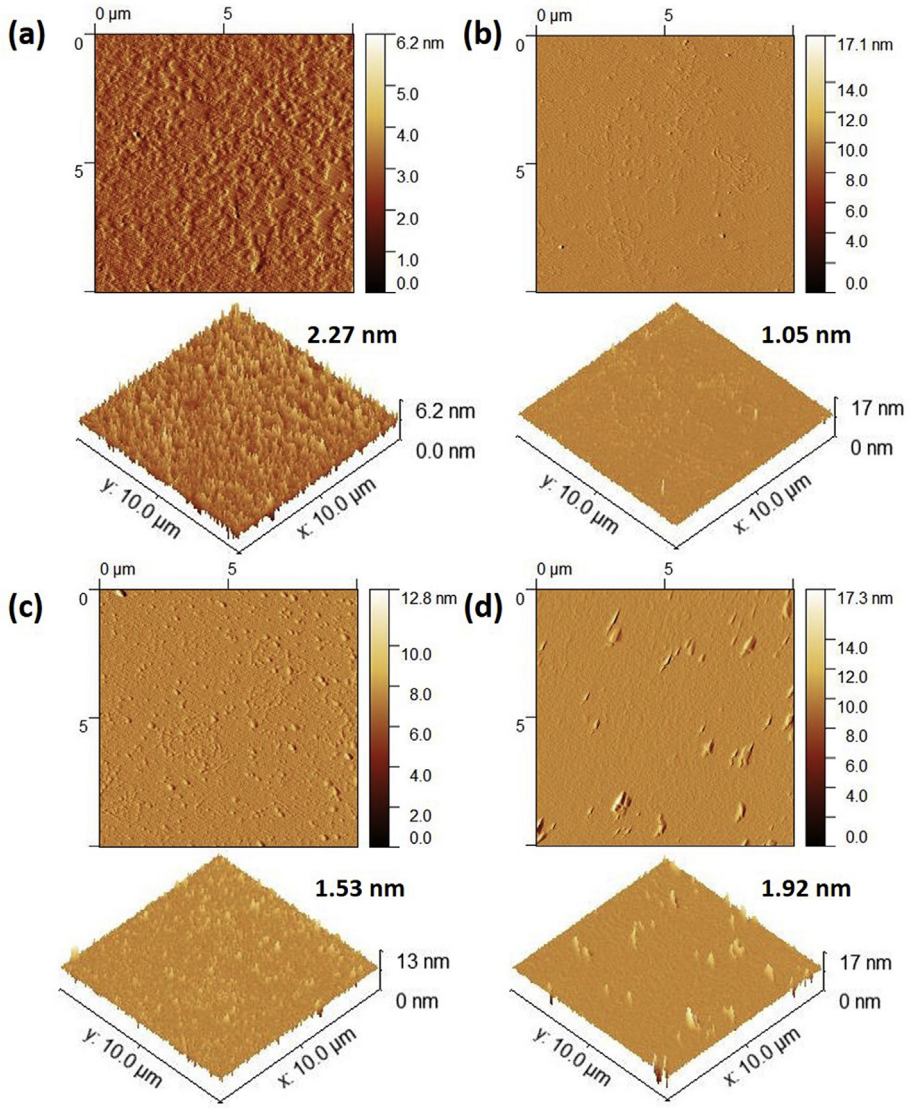

Fig. 4. Representative TM-AFM 2D and 3D topography images of (a) 7-7-7, (b) 7-11-7, (c) 7-15-7 and (d) 8-15-8. RMS values were given as inset.

wave, perpendicular to the sample, to ensure that there is enough space between the sample and the waveguides.

3. Results and discussion

The crystal structure plays an important role on the optical and electrical characteristics of the prepared thin films. Fig. 1 shows the GIXRD patterns of the films deposited with different stacking sequences onto PC. Peaks located at 30.1 ± 0.05° and 35.00 ± 0.05° can be indexed to the (222) and (400) planes of ITO with bixbyite crystal structure (JCPDS File No. 89–4596). No peak belonging to SnO or SnO_2 was detected. It is previously reported that the polycrystalline ITO films are only obtained when the substrate is heated up during deposition or annealing the film after deposition [24]. However, the existence of both (100) and (111) family of planes indicates the polycrystalline nature of the films that were grown in the absence of substrate heating. While ITO films deposited by various techniques are often reported to orient in [111] direction [25], preferred orientations on (400) and (622) planes were observed in ITO/Au/ITO multi-layer films on PC substrate. Although ITO thin films, grown under pure Ar, were reported to have a preferential (400) plane orientation, (222) plane orientation was observed in this study in the absence of gold as can be seen in Fig. 1 (b). Therefore, the (400) plane orientation of the films in this work is attributed to the introduction of Au interlayer. Furthermore, (400) plane of ITO possesses a lower surface energy compared to (222) plane. Once the (400) plane-oriented crystals are formed on the Au interlayer, the film would grow preferentially using the firstly formed (400) plane-oriented crystals as seed [26,27]. Since the ITO films grown at RT do not have sufficient activation energy for the Sn to substitute at the In sites, many of the Sn^{+2} cations sit in the films as an interstitial ion which leads to a higher interplanar spacing [28,29]. Therefore, 2θ shifts to lower values according to Bragg's law. Increasing interplanar spacing suggests elongation of unit cell along the a-axis of ITO which might result in the buildup of in-plane compressive stresses. Au (111) peak is obvious for the bilayer sample which consists 3 s Au deposition onto ITO layer without a top coat as indicated in Fig. 1 (a) (JCPDS File No. 04–0784). The broadening of the Au (111) peak might indicate that the deposited Au was in the form of nanoparticles, instead of a continuous film. Although the deposition duration of Au was short, the intensity of (111) peak of Au was stronger than ITO (222) plane. Relatively low intensity of ITO (222) plane was ascribed to the low crystallinity of the film, as it was deposited on polished PC at RT without a subsequent thermal annealing. Fig. 1 (b) shows that double layer deposition of ITO for 7 min, without an Au interlayer, also resulted in a low crystallinity. Nevertheless, (222) plane of ITO had a higher intensity when compared to the sample 7-3-0. Furthermore, ITO (440) plane also appeared as

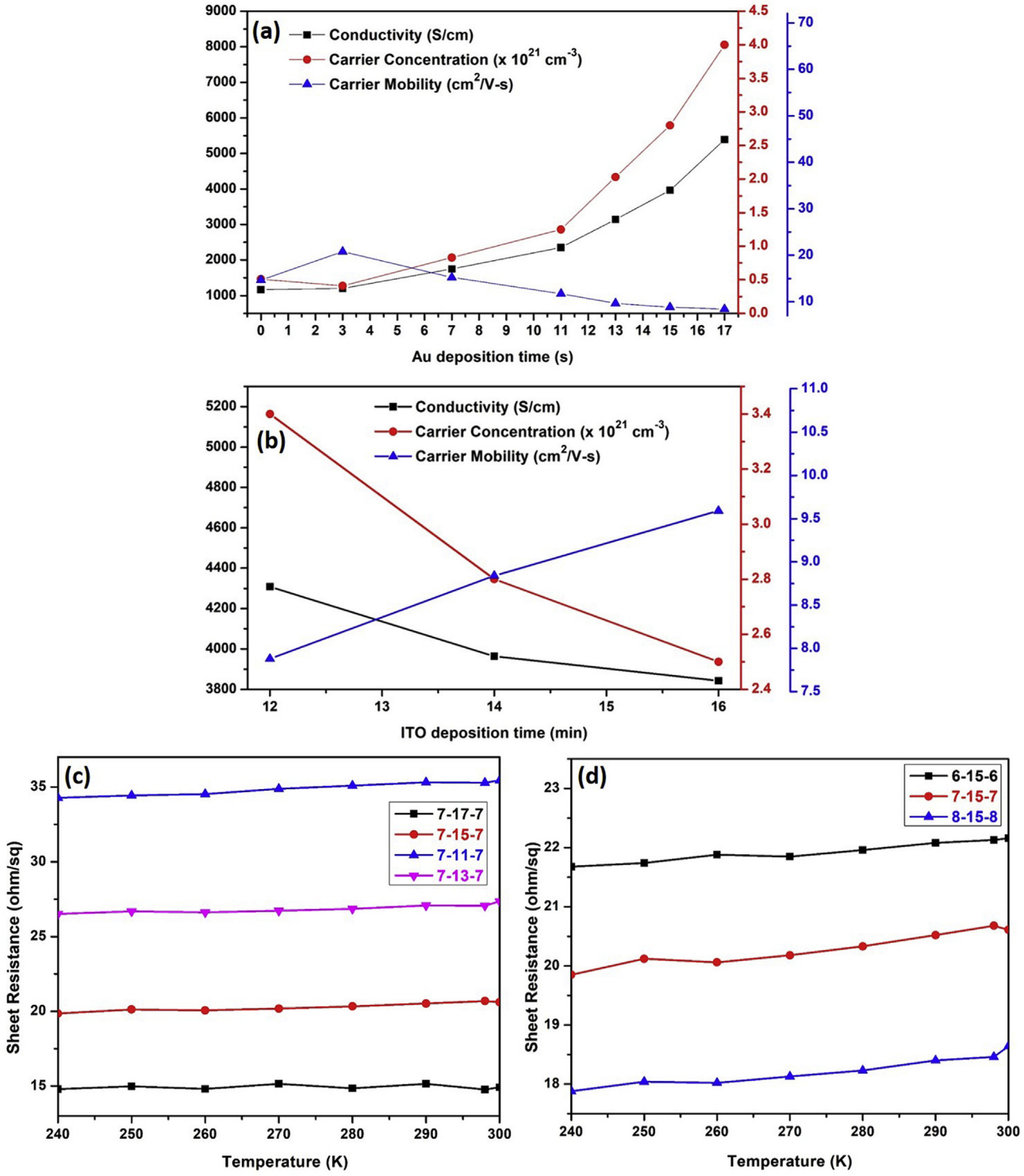

Fig. 5. Conductivity, carrier concentration and carrier mobility of thin films deposited onto SLG with respect to (a) Au deposition time, (b) ITO deposition time and temperature dependence of sheet resistance of thin films deposited on PC by changing (c) Au deposition time and (d) ITO deposition time.

indicated in Fig. 1 (b). The crystallinity increased due to thickening of the film with the deposition of top ITO layer which has a partial crystalline structure. Bilayer ITO deposited on PC without Au interlayer was observed to orient through [111] direction.

Fig. 1 (c) depicts the XRD pattern of 7-3-7 with an Au deposition of 3s. Crystallinity of ITO top layer considerably improved with the presence of Au. The intensity of (222) plane of ITO decreased rapidly. Further increase of Au deposition time to 11 s slightly enhanced crystallinity as shown in the XRD pattern of 7-11-7 in Fig. 1 (d). It should be noted that Au (111) peak is not clear in Fig. 1 (c) and (d) because of the very high intensities of ITO peaks as a result of increased crystallinity. The presence of Au (111) plane was clear upon closer inspection of the related part of the diffractograms. As the Au deposition time increased to 15 s, the (111) peak of Au became visible and ITO (400) and (622) peaks sharpened as can be seen in Fig. 1 (e).

SIMS analysis was conducted to investigate the elemental

Table 2
Highest optical transmittance (T_{max}) and electrical properties of films deposited on SLG.

Coding	T_{max} at 550 nm (%)	Conductivity (S/cm)	Carrier mobility (cm^2/V-s)	Carrier concentration (cm^{-3})	Sheet resistance (ohm/sq)
7-0-7	83.4	1165	14.68	$5.10x10^{20}$	83.27
7-3-7	81.0	1203	20.77	$4.12x10^{20}$	72.90
7-7-7	79.1	1750	15.24	$8.31x10^{20}$	49.25
7-11-7	81.6	2351	11.74	$1.25x10^{21}$	35.29
7-13-7	82.4	3143	9.67	$2.03x10^{21}$	27.07
7-15-7	84.6	3964	8.84	$2.80x10^{21}$	20.68
7-17-7	82.4	5391	8.41	$4.00x10^{21}$	14.77
6-15-6	81.3	4308	7.88	$3.40x10^{21}$	22.13
8-15-8	83.2	3842	9.59	$2.50x10^{21}$	18.46

distribution along the vertical path of the multilayers. SIMS depth profiles of samples 7-3-7 and 7-15-7 are shown in Fig. 2. As can be seen, the main elements of the ITO layers are In and Sn, the distribution of the two elements was uniform in the vertical direction. On the other hand, Au content increased quickly at a depth of around 50 nm as shown in Fig. 2 (a) and (b), which indicated the end of first ITO layer, and the beginning of Au interlayer. There is no significant interfacial reaction or diffusion between ITO and Au layers as the films were deposited at RT. It is found from Fig. 2 that Sn signal was much weaker in the spectrum of sample 7-3-7 than that of sample 7-15-7. Although the deposition times were equal, the presence of higher amounts of Au probably eased the deposition of Sn and increased its amount in the top ITO film. In line with the expectation, the area under the Au peak was greater in the sample 7-15-7 compared to 7-3-7 when the background is excluded.

Fig. 3 shows cross section and surface FESEM analyses of the films deposited onto SLG without additional coating. The representative FESEM cross section images given in Fig. 3 (a)–(c), showed that the thickness of the deposited films was uniform. Although the deposition was conducted at RT, the films did not delaminate during cutting. As expected, the interlayer could not be identified due to the limited detection of FESEM analysis. Yet, the thickness measurement on FESEM image was in good accordance with the surface profilometer result of sample 7-7-7, as shown in Fig. 3 (a) and given in Table S2.

Furthermore, the films exhibited a smooth surface morphology without any observable defects and/or cracks. Some lighter grains were monitored in the surface morphology of sample 7-7-7 and 7-15-7 as can be seen in Fig. 3 (d) and (e). The lighter grains are possibly the first crystallized grains during deposition. Moreover, no grain growth is identified in the FESEM image of sample 8-15-8 as shown in Fig. 3 (e). Fig. 3 (g) and Fig. 3 (h) show the HRTEM images of sample 6-15-6 at different magnifications. EDX spectrum taken during TEM is shown in Fig. S2. Thickness of the Au layer, in-between the ITO layers, was about 9 nm as indicated in Fig. 3 (h). The high-magnification TEM image in Fig. 3 (i), represented that the (400) lattice fringes of 2.57 Å period were parallel to the longitudinal axis of the top ITO layer. This means that the top ITO layer grew along the (400) plane, confirming previously shown XRD results.

Fig. 4 shows the representative TM-AFM 2D and 3D topography images (10 μm × 10 μm) of the representative samples. RMS roughness values ranging between 1 and 3 nm were calculated by processing AFM topography images. Fig. 4 (a) shows the 2D and 3D topography of sample 7-7-7. The highest RMS (2.27 nm) was calculated for this sample and this may indicate the formation of Au aggregates among the ITO layers. Au deposition is challenging due to its tendency to form islands instead of a continuous film. It is previously reported that the gold particles form disconnected island due to their surface diffusion in the early stages of the gold deposition by different fabrication methods [17]. The sizes of islands increase and then they coalesce to form a network by continued deposition. A cross section TEM image of sample 7-7-7 marking an Au aggregate is given in Fig. S3. Moreover, delamination of sandwich structure during FIB litography was observed in sample 7-7-7 probably due to inhomogeneous Au deposition as shown in Fig. S3. On the other hand, sample 7-11-7 showed the lowest RMS with 1.05 nm as depicted in Fig. 4 (b) which might indicate the formation of the interlayer film. Increasing the deposition time of Au caused higher roughness (1.53 nm) as evident in Fig. 4 (c) for 7-15-7. Fig. 4 (d) depicts topography of sample 8-15-8. The RMS roughness increased to 1.92 nm by increasing ITO deposition time. The roughness results obtained by AFM analyses were close to those given in literature [30,31] but slightly higher. Higher RMS roughness might be related to DC magnetron sputtering method used in this study instead of RF [29]. RT deposition and preferential orientation along (100) plane also contributes to roughness [32].

The electrical properties of D/M/D films are vital regarding to their EMI shielding behavior as well as optical performance. In general, the electrical conductivity of ITO films depends on the carrier mobility and the carrier density, which are mainly determined by oxygen vacancies or concentration of substituted Sn^{4+} on In^{3+} sites [30]. Variation of electrical conductivity, carrier concentration and carrier mobility with respect to the deposition times of Au and ITO onto SLG are given in Fig. 5 (a) and (b), respectively. All results that were calculated using the PPMS data are listed in Table 2. Sheet resistance was found to decrease by increasing both Au and ITO deposition time. Although carrier concentration decreased in sample 7-3-7 when compared to 7-0-7, it started to increase by further increasing of Au sputtering time.

Decrease of the charge carrier concentration with the first Au insertion is probably related to the increasing crystallinity of top layer. The introduced of Au interlayer behaved as nucleation sites for well-crystalline ITO deposition. Defects inside the relatively amorphous 7-0-7 may provide higher amount of carrier concentration [33] and short deposition time (3s) resulting in very small amount of Au inside the film may not contribute to carrier concentration effectively. Furthermore, preferential orientation of ITO through (100) plane after Au insertion may be effective on the decrease of carrier concentration. Thilakan et al. [34] suggested that (100) plane-oriented ITO films had better conductivity and carrier mobility compared to (111) plane-oriented films. Similarly, carrier mobility decreased with the increase in Au deposition time with the same exception. Since higher carrier concentration results in lower mobility and vice versa, sample 7-0-7 had lower mobility compared to 7-3-7.

Upon further increase of Au deposition, carrier mobility decreased sharply. The sharp decline of mobility may be related to the interface formation as well as increased charge carrier concentration. Decreasing rate of mobility slowed down after 11 s Au deposition, at which the film probably transited to bulk structure after completion of continuous film formation [15]. Moreover, the increase of ITO deposition time leads to a decrease in charge carrier concentration by decreasing Au proportion in the D/M/D films. Carrier mobility increases by increasing deposition time of ITO due to increase of bulk structure as well as reduced carrier concentration. As the decrease of charge carrier concentration was slightly higher compared to the increase of mobility, conductivity gently decreased as indicated in Fig. 5 (b). Fig. 5 (c) and (d) show variation of sheet resistance of D/M/D films deposited on PC substrate with temperature in the range between 240 and 300 K. It was found that sheet resistance variation of multilayer D/M/D films was negligible between 240 and 300 K. Sheet resistance distribution of single layer ITO film along the surface of PC substrate is also given in Fig. S4.

Fig. 6 (a) and (b) demonstrate the optical transmittance of representative D/M/D films deposited onto SLG and PC substrates, respectively. Transmittance was analyzed at RT in the 200–2500 nm wavelength range. Visible light transmittance graphs from 400 to 700 nm are also given as inset images in Fig. 6. Overall transmittance at 550 nm is given in Table 2. Optical transmittance enhanced by increasing ITO deposition time which improved the degree of crystallinity. Intercalation of Au layer decreased the transparency as indicated

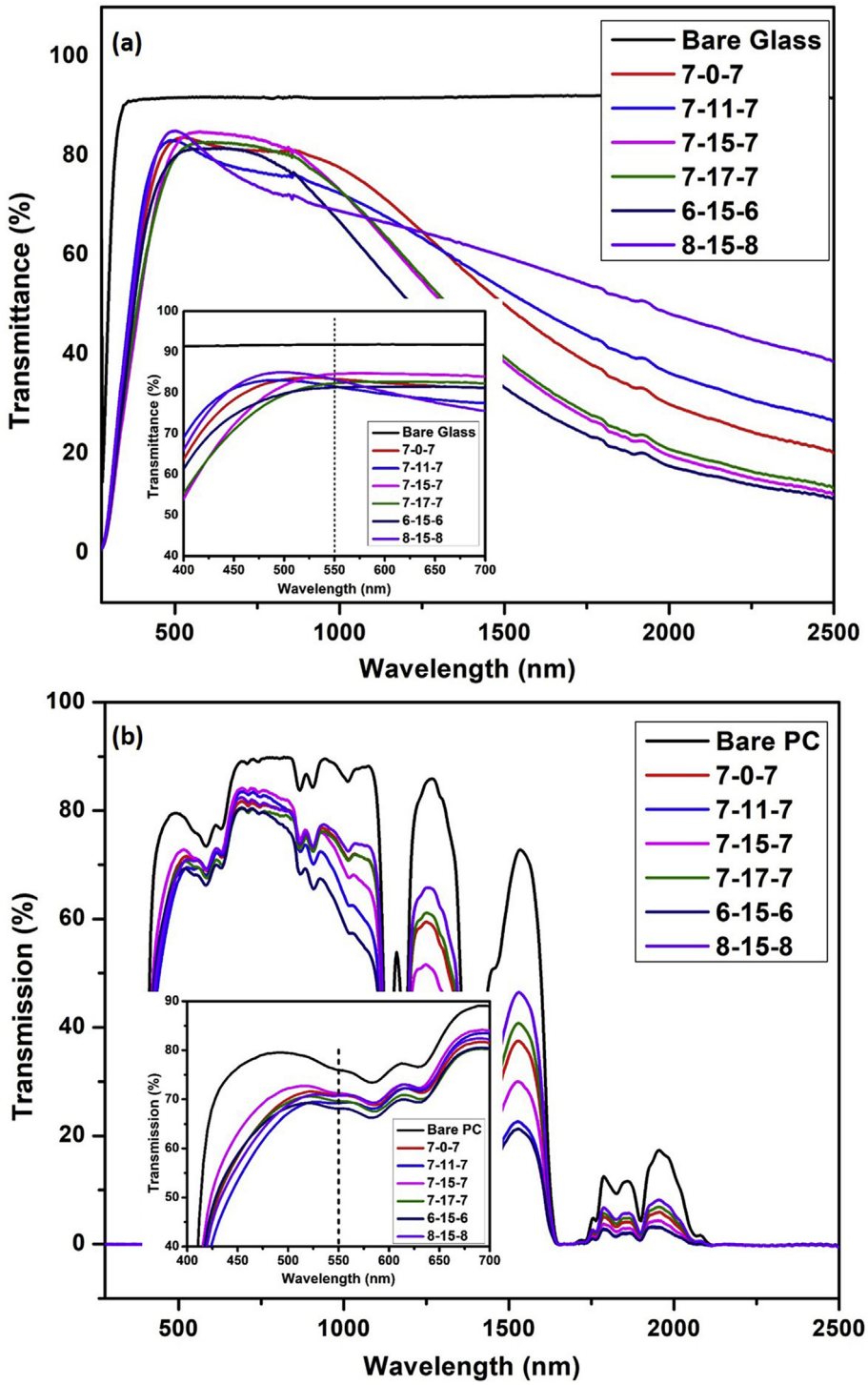

Fig. 6. Representative optical transmission spectra of D/M/D films deposited onto (a) SLG and (b) PC.

in Table 2. Several studies suggested that below a particular thickness of metal layer (Ag, Au, etc.), D/M/D multilayer films show fairly high sheet resistance and low optical transmittance due to unconnected metal islands and severe scattering due to these islands [22,35]. As-deposited multilayer films containing a gold interlayer with a deposition time of 15 s had the highest optical transmittance value, 84.6, as shown in Fig. 6 (b). The transparency at 550 nm decreased to 82.5% with further increase of Au deposition time. Although morphological and electrical characterization suggested well-connected film formation in sample 7-11-7, further increase of Au deposition time resulted in higher transparency at 550 nm. Optical analyses indicated that continuous film formation with the highest transmittance and lowest scattering obtained at Au deposition time of 15 s. In general, surface plasmonics on the Au film causes reflectance of light [31]. However, D/M/D structure with continuous metal film transmits visible light more than the bi-layer film of ITO as given in Table 2. Optical transmittance first increased and then decreased by increasing ITO deposition time as shown in Fig. 6. It is known that optical transmittance is strongly related to the charge carrier concentration [36]. Accordingly, higher amount of carrier concentration in sample 6-15-6 lead to a lower optical

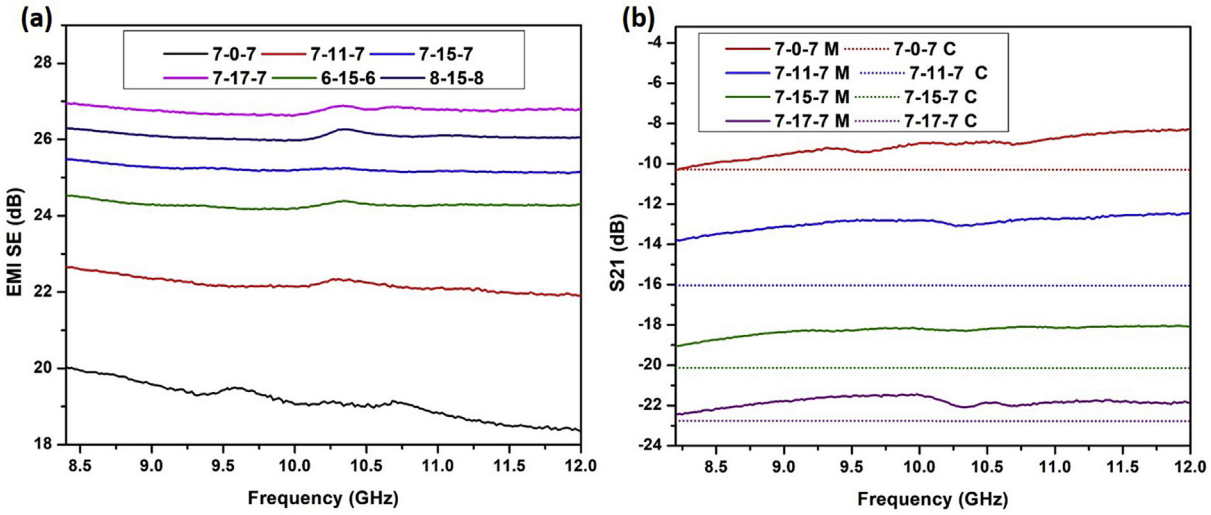

Fig. 7. (a) Measured EMI SE values of representative samples and (b) Measured and simulated S_{21} values of the samples. M: Measured and C: Calculated.

Table 3
Measured and simulated average EMI SE of samples between 8 and 12 GHz and highest optical transmittance of D/M/D films deposited on PC substrate.

Sample	Simulated EMI SE (dB)	Simulated S_{21} (dB)	Measured S_{21} (dB)	Measured EMI SE (dB)	Power Attenuation %	T_{max} at 550 nm (%)
7-0-7	20.3	−10.3	−9.1	19.2	98.8	70.8
7-11-7	24.1	−16.0	−12.9	22.2	99.4	69.2
7-15-7	26.1	−20.1	−18.3	25.2	99.7	71.2
7-17-7	27.2	−22.8	−21.8	26.8	99.8	69.6
6-15-6	25.8	−19.5	−16.4	24.3	99.6	68.0
8-15-8	26.5	−21.0	−21.7	26.1	99.8	70.3

transmittance. Maximum optical transmittance (T_{max}) was achieved by sample 7-15-7 as indicated in Fig. 6. Further increase of ITO deposition is found to decrease transparency due to thickening of the ITO film (see Table S2). The optical transparency order of samples at 550 nm did not change for PC and glass substrates. Nevertheless, the transparency values and overall transparency changed noticeably in different substrates.

EMI SE of the prepared D/M/D films were measured between 8 and 12 GHz, as shown in Fig. 7 (a) and Table 3. It is evident from the figure that as-prepared D/M/D films provided an efficient shielding in the widely used X-band. The primary mechanism of EMI shielding was reflection of radiation through the mobile charge carriers (electrons and/or holes). Moreover, a second mechanism was the absorption by the electric and/or magnetic dipole of shielding materials.

ITO has a relatively low dielectric constant for the absorption of radiation. EMI shielding performance of ITO is known to be strongly depending on the sheet resistance and charge carrier concentration [37]. Moreover, multiple internal reflections are often neglected when EMI SE is more than 15 dB. From the above reasons, reflection is the dominant factor on the EMI shielding performances of D/M/D films, and therefore, they can be used in transparent EMI shielding applications by proper control of the electrical properties. As shown in Table 3, Sample 7-17-7 with the lowest R_s and the highest charge carrier concentration, as well as the best conductivity showed excellent EMI shielding performance approaching to 27 dB, which performed 99.8% power attenuation. Moreover, EMI shielding performance was found to decrease by increasing R_s for all of the conditions tested. When the ITO content is constant, EMI shielding performance tended to increase with carrier concentration as can be seen in Table 3, where adding more Au resulted in better shielding. On the other hand, R_s seemed to govern the shielding behavior for varying ITO thicknesses, rather than carrier concentration. For instance, although 7-15-7 possessed higher carrier concentration, 8-15-8 yielded better shielding, thanks to its lower R_s value. Likewise, the lowest EMI SE was measured with sample 7-0-7 which possessed the highest R_s and the lowest conductivity. The results strongly indicated the importance of sheet resistance on the EMI shielding performance of sandwich structures.

Finally, measured S_{21} parameters were compared with the theoretically calculated S_{21} values in the range of 8–12 GHz using commercial CST microwave software as depicted in Fig. 7 (b). Normally, a linear S_{21} and EMI SE data are expected through the frequency range in the case of a smooth thin film, which was the case for simulated data as shown in Fig. 7 (b). There is a negligible noise in the measured plots and the difference between the simulated and measured ones was inherently caused by the mismatch in connectors and natural behavior of electrical switching mechanism and harmonics [38]. The higher deviation of measurement for 7-11-7 from the simulation might have been caused by incomplete Au layer due to shorter deposition time.

4. Conclusions

D/M/D sandwich coatings, which greatly relieves the trade-off between visible light transparency and EMI shielding, were successfully prepared by magnetron sputtering. Unlike most of the previous studies, the sputtering was conducted in the absence of substrate heating as PC substrates were used to converge industrial application. It was found that the presence of the metal interlayer improved the electrical conductivity and the optical transparency significantly by tailoring crystallinity and morphology of the film. Moreover, we report that even discontinuous Au interlayer in island-like structure, greatly improved ITO crystallinity. On the other hand, preferential orientation through (400) caused by intercalation of Au did not influence the electrical properties of the D/M/D film. By optimizing the gold deposition time, the sample with the best optical transparency was obtained at 15 s deposition duration. In addition, deposition time of ITO was optimized for the lowest sheet resistance without causing a significant decrease of the carrier mobility. The EMI SE results of both measured and simulated data showed power attenuation values ranging between 98.8 and

99.8%. Overall, the ITO/Au/ITO sandwich films deposited on PC substrate possessed successful EMI shielding results. We believe development of novel robust films with higher conductivity and transparency can make significant scientific contributions to EMI shielding studies in the future.

Declaration of competing interest

The authors declare that they have no known competing financial interests or personal relationships that could have appeared to influence the work reported in this paper.

Acknowledgement

This work was partially supported by Scientific and Technological Research Council of Turkey (TUBİTAK) under contract number of 5189901 and Turkish Aerospace. The authors thank to the collaboration between Turkish Aerospace and Bilkent University Institute of Materials Science and Nanotechnology (UNAM). The authors also thank to Enver Kahveci and Mustafa Guler for the assistance in the GIXRD and FIB litography, respectively. The authors are indebted to Dr. H. Volkan Demir and Dr. Metehan Erdogan for their critical scientific recommendations.

Appendix A. Supplementary data

Supplementary data to this article can be found online at https://doi.org/10.1016/j.cap.2020.01.012.

References

[1] X. Yu, T.J. Marks, A. Facchetti, Metal oxides for optoelectronic applications, Nat. Mater. 15 (2016) 383–396, https://doi.org/10.1038/nmat4599.
[2] H.L. Hartnagel, A.L. Dawar, A.K. Jain, G. Jagdish, Semiconducting, Transparent Thin Film, IOP Publishing, Bristol and Philadelphia, 1995.
[3] T. Yamada, T. Morizane, T. Arimitsu, A. Miyake, H. Makino, N. Yamamoto, T. Yamamoto, Application of low resistivity Ga-doped ZnO films to transparent electromagnetic interference shielding material, Thin Solid Films 517 (2008) 1027–1031, https://doi.org/10.1016/j.tsf.2008.06.047.
[4] E.-H. Ko, H.-J. Kim, S.-J. Lee, J.-H. Lee, H.-K. Kim, Nano-sized Ag inserted into ITO films prepared by continuous roll-to-roll sputtering for high-performance, flexible, transparent film heaters, RSC Adv. 6 (2016) 46634–46642, https://doi.org/10.1039/C6RA08704C.
[5] N. Al-Dahoudi, H. Bisht, C. Gobbert, T. Krajewski, M.A. Aegerter, Transparent conducting, anti-static and anti-static–anti-glare coatings on plastic substrates, Thin Solid Films 392 (2001) 299–304, https://doi.org/10.1016/S0040-6090(01)01047-1.
[6] D.-P. Tran, H.-I. Lu, C.-K. Lin, Conductive characteristics of Indium Tin Oxide thin film on polymeric substrate under long-term static deformation, Coatings 8 (2018) 212, https://doi.org/10.3390/coatings8060212.
[7] N.R. Armstrong, P.A. Veneman, E. Ratcliff, D. Placencia, M. Brumbach, Oxide contacts in organic photovoltaics: characterization and control of near-surface composition in Indium − Tin Oxide (ITO) electrodes, Acc. Chem. Res. 42 (2009), https://doi.org/10.1021/ar900096f 1748-17.
[8] J.J. Lee, J.S. Kim, S.J. Yoon, Y.S. Cho, J.W. Choi, Electrical and optical properties of Indium Zinc Oxide (IZO) thin films by continuous composition spread, J. Nanosci. Nanotechnol. 13 (2013) 3317–3320, https://doi.org/10.1166/jnn.2013.7274.
[9] E. Muchuweni, T.S. Sathiaraj, H. Nyakotyo, Effect of gallium doping on the structural, optical and electrical properties of zinc oxide thin films prepared by spray pyrolysis, Ceram. Int. 42 (2016) 10066–10070, https://doi.org/10.1016/j.ceramint.2016.03.110.
[10] A. Eshaghi, M. Hajkarimi, Optical and electrical properties of aluminum zinc oxide (AZO) nanostructured thin film deposited on polycarbonate substrate, Optik 125 (2014) 5746–5749, https://doi.org/10.1016/j.ijleo.2014.07.056.
[11] F. Turkoglu, H. Koseoglu, S. Zeybek, M. Ozdemir, G. Aygun, L. Ozyuzer, Effect of substrate rotation speed and off-center deposition on the structural, optical, and electrical properties of AZO thin films fabricated by DC magnetron sputtering, J. Appl. Phys. 123 (2018) 165104, https://doi.org/10.1063/1.5012883.
[12] K. Suzuki, N. Hashimoto, T. Oyama, J. Shimizu, Y. Akao, H. Kojima, Large scale and low resistance ITO films formed at high deposition rates, Thin Solid Films 226 (1993) 104, https://doi.org/10.1016/0040-6090(93)90213-9.
[13] C. Guillén, J. Herrero, TCO/metal/TCO structures for energy and flexible electronics, Thin Solid Films 520 (2011) 1–17, https://doi.org/10.1016/j.tsf.2011.06.091.
[14] H. Zhou, J. Xie, M. Mai, J. Wang, X. Shen, S. Wang, L. Zhang, K. Kisslinger, H.Q. Wang, J. Zhang, Y. Li, J. Deng, S. Ke, X. Zeng, High-quality AZO/Au/AZO sandwich film with ultralow optical loss and resistivity for transparent flexible electrodes, ACS Appl. Mater. Interfaces 9 (2018) 16160–16168, https://doi.org/10.1021/acsami.8b00685.
[15] X. Fang, C. Leung Mak, J. Dai, K. Li, H. Ye, C.W. Leung, ITO/Au/ITO sandwich structure for near-infrared plasmonics, ACS Appl. Mater. Interfaces 6 (2014) 15743–15752, https://doi.org/10.1021/am5026165.
[16] F. Vigneron, V. Caps, Evolution in the chemical making of gold oxidation catalysts, C. R. Chimie 19 (2016) 192–198, https://doi.org/10.1016/j.crci.2015.11.015.
[17] Y. Lee, D. Kim, J. Jeong, J. Kim, V. Shmid, O. Korotchenkov, P. Vasa, Y.-M. Bahk, D.-S. Kim, Enhanced terahertz conductivity in ultra-thin gold film deposited onto (3-mercaptopropyl) trimethoxysilane (MPTMS)-coated Si substrates, Sci. Rep. 9 (2019) 15025, https://doi.org/10.1038/s41598-019-51085-0.
[18] A. Sytchkova, M.L. Grilli, A. Rinaldi, S. Vedraine, P. Torchio, A. Piegari, F. Flory, Radio frequency sputtered Al:ZnO-Ag transparent conductor: a plasmonic nanostructure with enhanced optical and electrical properties, J. Appl. Phys. 114 (2013) 094509, , https://doi.org/10.1063/1.4820266.
[19] J.T. Guske, J. Brown, A. Welsh, S. Franzen, Infrared surface plasmon resonance of AZO-Ag-AZO sandwich thin films, Optic Express 20 (2012) 23215–23226, https://doi.org/10.1364/OE.20.023215.
[20] R.A. Maniyara, V.K. Mkhitaryan, T.L. Chen, D.S. Ghosh, V. Pruneri, An antireflection transparent conductor with ultralow optical loss (< 2 %) and electrical resistance (< 6 Ω sq − 1), Nature comm 7 (2016) 13771, https://doi.org/10.1038/ncomms13771.
[21] S.-M. Lee, H.-W. Koo, T.-W. Kim, H.-K. Kim, Asymmetric ITO/Ag/ZTO and ZTO/Ag/ITO anodes prepared by roll to roll sputtering for flexible organic light-emitting diodes, Surf. Coating. Technol. 343 (2018) 115–120, https://doi.org/10.1016/j.surfcoat.2017.10.048.
[22] O. Tuna, Y. Selamet, G. Aygun, L. Ozyuzer, High quality ITO thin films grown by DC and RF sputtering without oxygen, J. Phys. D Appl. Phys. 43 (2010) 055402, , https://doi.org/10.1088/0022-3727/43/5/055402.
[23] ASTM D5568-14, Standard Test Method for Measuring Relative Complex Permittivityand Relative Magnetic Permeability of Solid Materials at Microwave Frequencies Using Waveguide, ASTM International, West Conshohocken, PA, 2014, https://doi.org/10.1520/D5568-14.
[24] Y. Jung, Y. Choi, H. Lee, D. Lee, Effects of thermal treatment on the electrical and optical properties of Silver-based Indium Tin Oxide/metal/Indium Tin Oxide structures, Thin Solid Films 440 (2003) 278, https://doi.org/10.1016/S0040-6090(03)00835-6.
[25] L. Dong, S. Zhu, H.R. Xu, X.P. Jiang, X.Y. Zhang, Y.Y. Zhao, D.L. Yan, L. Yuan, A.B. Yu, Preparation of Indium Tin Oxide (ITO) thin film with (400) preferred orientation by sol–gel spin coating method, J. Mater. Sci. Mater. Electron. 30 (2019) 8047–8054, https://doi.org/10.1007/s10854-019-01126-1.
[26] J. Lee, M.A. Petruska, S. Sun, Surface modification and assembly of transparent Indium Tin Oxide nanocrystals for enhanced conductivity, J. Phys. Chem. C 118 (2014) 12017–120219, https://doi.org/10.1021/jp502361d.
[27] L. Meng, M.P. Santos, Properties of Indium Tin Oxide films prepared by rf reactive magnetron sputtering at different substrate temperature, Thin Solid Films 322 (1998) 56–62, https://doi.org/10.1016/S0040-6090(97)00939-5.
[28] N.M. Ahmed, F.A. Sabah, H.I. Abdulgafour, A. Alsadig, A. Suliemane, M. Alkhoaryef, The effect of post annealing temperature on grain size of Indium-Tin-Oxide for optical and electrical properties improvement, Results in Physics 13 (2019) 102159, https://doi.org/10.1016/j.rinp.2019.102159.
[29] V. Sivaji Reddy, K. Das, A. Dhar, S.K. Ray, The effect of substrate temperature on the properties of ITO thin films for OLED applications, Semicond. Sci. Technol. 21 (2006) 1747–1752, https://doi.org/10.1088/0268-1242/21/12/043.
[30] Y.S. Kim, J.H. Park, D.H. Choi, H.S. Jang, J.H. Lee, H.J. Park, J.I. Choi, D.H. Ju, J.Y. Lee, D. Kim, ITO/Au/ITO multilayer thin films for transparent conducting electrode applications, Appl. Surf. Sci. 254 (2007) 1524–1527, https://doi.org/10.1016/j.apsusc.2007.07.080.
[31] W. Wei, R. Hong, J. Wang, C. Tao, D. Zhang, Electron-beam irradiation induced optical transmittance enhancement for Au/ITO and ITO/Au/ITO multilayer thin films, J. Mater. Sci. Technol. 33 (2017) 1107–1112, https://doi.org/10.1016/j.jmst.2017.07.006.
[32] D. Kim, Characterization of low pressure annealed ITO/Au/ITO films prepared by reactive magnetron sputtering, J. Alloys Compd. 493 (2010) 208–211, https://doi.org/10.1016/j.jallcom.2009.12.056.
[33] J.R. Bellingham, Electrical and optical properties of amorphous Indium Oxide, J. Phys. Condens. Matter 2 (1990) 6207, https://doi.org/10.1088/0953-8984/2/28/011.
[34] P. Thilakan, J. Kumar, Studies on the preferred orientation changes and its influenced properties on IT0 thin films, Vacuum 48 (1997) 463–466, https://doi.org/10.1016/S0042-207X(96)00309-0.
[35] M. Lebioda, R. Pawlak, Influence of cryogenic temperatures on electrical properties of structures patterned by a laser in ITO/Ag/ITO layers, Phys. Status Solidi 213 (2016) 1150–1156, https://doi.org/10.1002/pssa.201532693.
[36] J.D. Perkins, J.A. del Cueto, J.L. Alleman, C. Warmsingh, B.M. Keyes, L.M. Gedvilas, P.A. Parilla, B. To, D.W. Readey, D.S. Ginley, Combinatorial studies of Zn-Al-O and Zn-Sn-O transparent conducting oxide thin films, Thin Solid Films 411 (2002) 152–160, https://doi.org/10.1016/S0040-6090(02)00205-5.
[37] Y.-J. Choi, S.C. Gong, D.C. Johnson, S. Golledge, G.Y. Yeom, H.-H. Park, Characteristics of the electromagnetic interference shielding effectiveness of Al-doped ZnO thin films deposited by atomic layer deposition, Appl. Surf. Sci. 269 (2013) 92–97, https://doi.org/10.1016/j.apsusc.2012.09.159.
[38] R. Pettai, Noise in Receiving Systems, Wiley, Newyork, 1984.